Heritage Science

RESEARCH

Open Access

Formation mechanism of copper-gilded coronet ornaments excavated from a Sui or early Tang tomb situated in Xi'an, Shaanxi

Yanbing Shao[1], Fengrui Jiang[2,3*], Junchang Yang[1,3*], Quanmin Zhang[4], Xuan Lu[5], Wenbin Fu[5] and Sumei Yu[6]

Abstract

The formation of the gold layer in mercury gilding occurs through the heating a gold amalgam. As a result, the formation mechanism and technical characteristics of gilded products are closely related to the temperature at which they are heated. In this study, XRD and XPS analysis of a copper-gilded coronet from the *Sui* or *Tang* dynasties revealed that Au_3Cu was one of the main phases of the gold layer. Therefore, base on the thermodynamic stability of ordered phases like Au_3Cu, the estimated heating temperature for this copper-gilded coronet ranged from 240 to 285 ℃. Furthermore, SEM–EDS analysis of the cross-sectional concentration distribution of Cu indicated that the diffusion distance of Cu during heating did not exceed 2 μm. At 240–285 ℃, Cu diffused along the defects of the gold layer, and the diffusion process followed Fick's second law. Previous research has indicated that the defect path diffusion coefficient of Cu is on the order of 10^{-12} cm^2/s, and the heating time of the gilding process is typically considered to be 15 min. Using the diffusion equation, the calculated diffusion distance of Cu aligned with the diffusion behavior of Cu at 240–285 ℃, confirming the inferred heating temperature range. Additionally, at these temperatures, the gold layer was formed through the solid-state reaction of the gold amalgam and was bonded to the substrate through the diffusion of Cu.

Keywords Mercury gilding, Copper-gilded products, Au-Cu system, Au-Cu compounds, Diffusion coefficient, *Sui* and *Tang* dynasties

Introduction

Gold, one of the earliest precious materials used by ancient ancestors, has always symbolized wealth, prestige, and power [1]. This metal's enduring popularity can be attributed to its vibrant and long-lasting color, malleable texture, and ease of processing [2]. Given its rarity and value, civilizations throughout history have sought to replicate the appearance of gold [3, 4]. Consequently, in the fifth century BC or even earlier, techniques such as foil gilding (wrapping a silver or copper-based alloy with gold foil) and leaf gilding (gold plating with an adhesive) were invented [5, 6]. However, these gilding processes typically resulted in gold layers measuring 2–10 microns or even thicker, highlighting the need to conserve the use of gold [7–9]. As technologies for achieving gold-like

*Correspondence:
Fengrui Jiang
jiangfengrui@nwpu.edu.cn
Junchang Yang
yangjunchang@nwpu.edu.cn
[1] State Key Laboratory of Solidification Processing, Center for Nano Energy Materials, School of Materials Science and Engineering, Northwestern Polytechnical University, Xi'an 710072, China
[2] Construction Preparatory Office of Museum, Northwestern Polytechnical University, Xi'an 710072, China
[3] Institute of Culture and Heritage, Northwestern Polytechnical University, Xi'an 710072, China
[4] Xi'an Institute of Conservation and Archaeology On Cultural Heritage, Xi'an 710068, China
[5] Shaanxi History Museum (Shaanxi Cultural Relics Exchange Center), Xi'an 710061, China
[6] Duolun Cultural Relics Conservation Center, Xilingol League 026000, China

appearances advanced, the challenge emerged to utilize minimal quantities of gold across different cultures [10]. In China, during the fourth century BC, a novel gold decoration technique called mercury gilding or fire gilding emerged through the combination of gold and mercury [11, 12]. This technique earned its name *fire gilding* due to the essential heating step involved in the process. Unlike gold foil and gold leaf, the paste-like gold amalgam used in fire gilding provided a more seamless integration with the substrate [13]. Consequently, fire gilding not only resulted in thinner and superior gold layers [14] but also significantly reduced the consumption of gold in the process [15]. Therefore, it quickly became one of the most successful methods for ancient craftsmen to explore the effective utilization of precious and scarce resources [16–18]. In addition, owing to the utilization of amalgam, it is an indication of the technical advancement of ancient China.

At present, research on gilding processes is mainly based on ancient records. In fire gilding, gold amalgam is first coated on the surface of the base metal and then heated to form a gold film. During heating, most of the mercury is evaporated, leaving a porous gold layer [12, 19]. However, due to the solid solution reaction of Au and Hg, a small amount of mercury remains [20]. Even so, mercury is not a unique feature of fire gilding. As early as the fifth century BC to the fourth century BC, the people of the Eurasian grassland began to use mercury to stick the gold foil and gold sheets on ironware [21]. Therefore, scholars have conducted in-depth research on fire gilding to discover more technical features of this technology [22].

In recent years, more and more advanced material analysis methods and theories have been used for the research of cultural relics [23–25]. The heating process and formation mechanism of gilding technology have been deeply studied by analyzing the interface and phase composition of gilded items [26]. The gold layer is formed by the phase transformation of gold amalgam during heating. Consequently, the Au-Hg system has become a new research focus in fire gilding [27]. α-Au, which is only formed above 419 ℃, has been found in the gold layer of cultural relics. Thus, some scholars believe that the heating temperature of fire gilding is higher than 419 ℃ [28]. However, other scholars insist that mercury evaporates from the Au-Hg system during the gilding process and that the proportion of Au/Hg in this open system continuously changes. Hence, the whole process is a solid-state reaction process and does not involve the melting of Au-Hg alloy [27, 29]. In addition, the main purpose of this ancient gilding process is to obtain a golden surface layer that is firmly bonded to the substrate. Thus, the metalsmiths should take special care to avoid overheating these objects due to the tendency of copper to oxidize in the air at high temperatures [30]. Due to the porosity of gold amalgam, copper will be enriched beneath the gold, which is easily transformed into copper corrosives in the subsequent storage process [31, 32]. This phenomenon eventually causes the plating to flake off [33]. Hence, the heating temperature of this ancient gilding process is considered to be 250–350 ℃, which is lower than the boiling point of mercury (357 ℃) [12, 34]. Unfortunately, based on the study of Au-Hg system, no reasonable and consistent conclusions have been drawn on the heating temperature and formation mechanism of fire gilding.

In contrast to the extensive research conducted on the crystal structure of Au-Hg alloys, there has been limited focus on ancient gold alloys, particularly in the context of the crystal structure of Au-Cu alloys. However, in the case of copper-gilded relics, the influence of heating on diffusion and phase transformation within the Au-Cu system cannot be disregarded. Recent experimental findings have revealed the formation of an ordered phase within the Au-Cu system under specific conditions, particularly at intermediate temperatures ranging from 150 to 400 °C. Furthermore, heating promotes the rapid diffusion of copper atoms into the gold layer within the Au-Cu system [35]. Consequently, investigating the diffusion and phase composition of the Au-Cu system during the heating process presents a promising and viable research approach for examining the heating process and understanding the formation mechanism of fire gilding.

The end of the *Sui (隋)* Dynasty marked the conclusion of China's previous division, leading to the advent of the *Tang (唐)* Dynasty, which ushered in an unprecedented era of openness and prosperity [36]. With China's robust national strength, various ancient metal processing techniques reached their zenith during this period. The construction of exquisitely designed and intricate female gilded hair accessories became particularly prominent. For instance, the earliest gilt-copper beads emerged on the crown of Empress *Xiao (萧)*, which currently stands as the highest-ranking ceremonial crown. These beads, with a minimum diameter of merely 0.4 mm, were adorned with a gold layer of minimum thickness measuring 10 μm (Fig. 1a, b) [37]. Undeniably, gilding technology had reached its pinnacle of development and sophistication at this juncture. Consequently, exploring high-grade gilding products from this period can offer valuable insights into the technological advancements achieved during the heyday of gilding technology [38].

In this study, a collection of high-grade copper-gilded coronet ornaments, resembling the crown of Empress *Xiao* from the *Sui* or *Tang* dynasties, were carefully selected for comprehensive analysis [4]. Through an

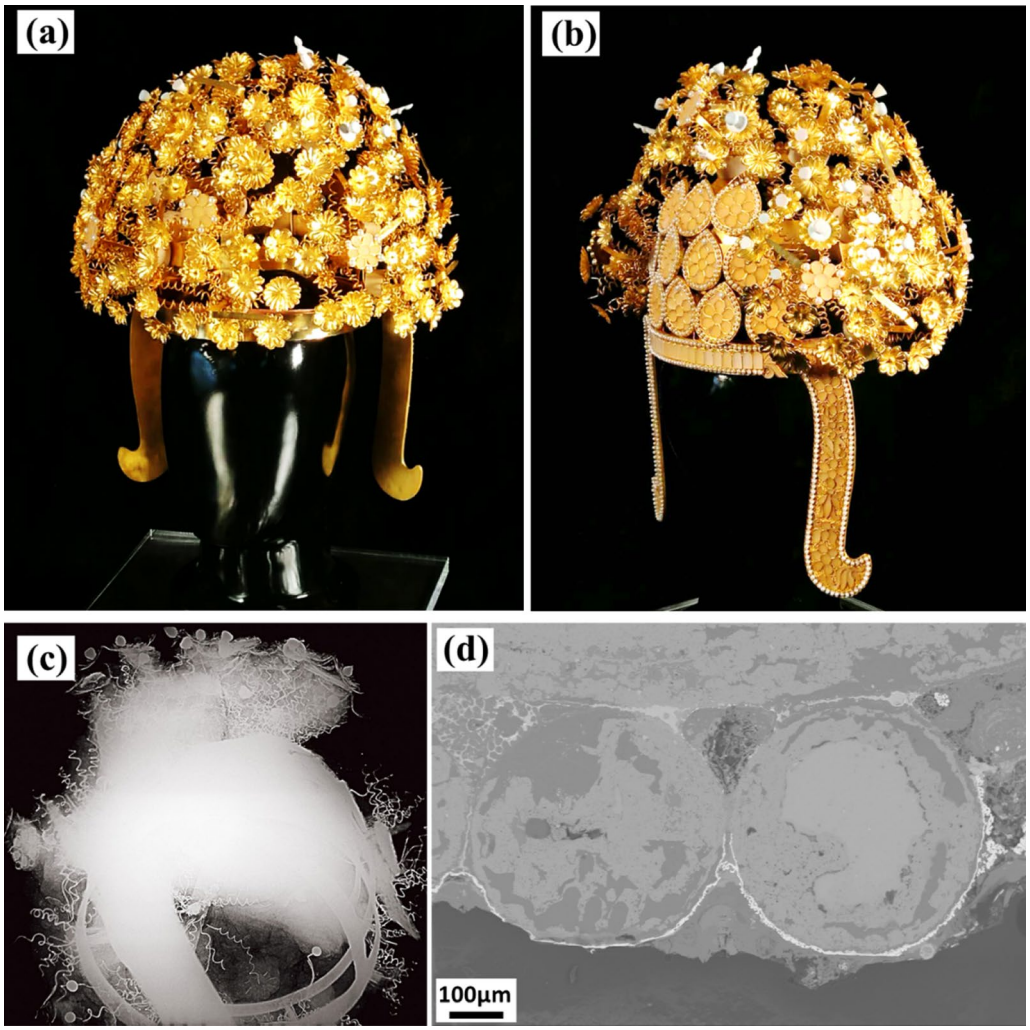

Fig. 1 Replica crown of Empress Xiao (**a**: front, **b**: side); X-ray image of ceremonial crown of Empress Xiao **c** [37]; BSE image of the gilt copper beads of the crown **d**

in-depth examination of the phase composition of the gold layer and the diffusion behavior of copper atoms, we aim to elucidate the formation mechanism during gilding and the bonding mechanism between the gold layer and the substrate. Such investigations will contribute to our understanding of the technological advancements attained during the gilding process and shed light on the underlying mechanisms involved in the bond formation between the gold layer and the substrate.

Materials

The gilded cultural relics were discovered in Tomb M2, located in *Xi'an (西安)*, *Shaanxi (陕西)*, China. Tomb M2consists of a single-chamber earth cave and a long ramped passage, indicative of its architectural structure [39]. The shape and structure of the tomb, along with the artifacts unearthed from it, suggest a potential association with the *Sui* Dynasty (581 – 618 CE) or, at the very least, a timeframe no later than the early *Tang* dynasty (7th – eighth century CE) [40]. Notably, during the excavation process, a collection of meticulously arranged gilded ornaments was found surrounding the head of the female tomb owner [41]. According to relevant research [39], these objects were identified as decorative components of a high-grade ceremonial coronet. As a result, Tomb M2 presents a valuable opportunity to explore ancient gilding technology and gain insights into this field of study.

The excavated coronet exhibited poor preservation, with significant degradation of all its components, making the original structure difficult to ascertain. However, after an initial cleaning process, it became apparent that

the coronet primarily consisted of two wing-shaped ornaments (referred to as temples) and eight apricot-leaf-shaped ornaments. These ornaments were embellished with pearls, glass, and various gemstones (see Fig. 2a). In addition to a multitude of metal ornaments shaped like petals, ties, water droplets, and leaves, the coronet also featured the presence of jade and mother-of-pearl (see Fig. 2b). During the period spanning the Sui and Tang dynasties (581–907 CE), the number of decorative ornaments adorning a coronet served as an indicator of the wearer's social status [41]. Hence, the presence of eight apricot leaf ornaments and two temples on this coronet suggests that it was a personal adornment worn by high-ranking females within the hierarchical system of that era [42]. The metal ornaments comprising the coronet displayed a visually captivating golden yellow surface. In order to ascertain the manufacturing process of this golden appearance, a thorough scientific analysis was conducted on all the metal components. To facilitate subsequent descriptions, abbreviations have been assigned to each specific component: TB represents the temple, SD represents the apricot leaf decoration, PS represents the petal decoration, TS represents the tie decoration, WS represents the droplet decoration, LS represents the leaf decoration, and CW represents the copper wire. To obtain the elemental and phase compositions of the gold layer in the coronet, non-destructive testing was employed on the provided samples. However, to explore the cross-sectional composition and structural characteristics of the components, the cross-sectional samples were prepared according to the following steps. Fragments (2 mm × 2 mm) were first cut from each sample, in-laid in the embedding resin (Buehler epoxy resin and Buehler epoxy hardener), ground using abrasive

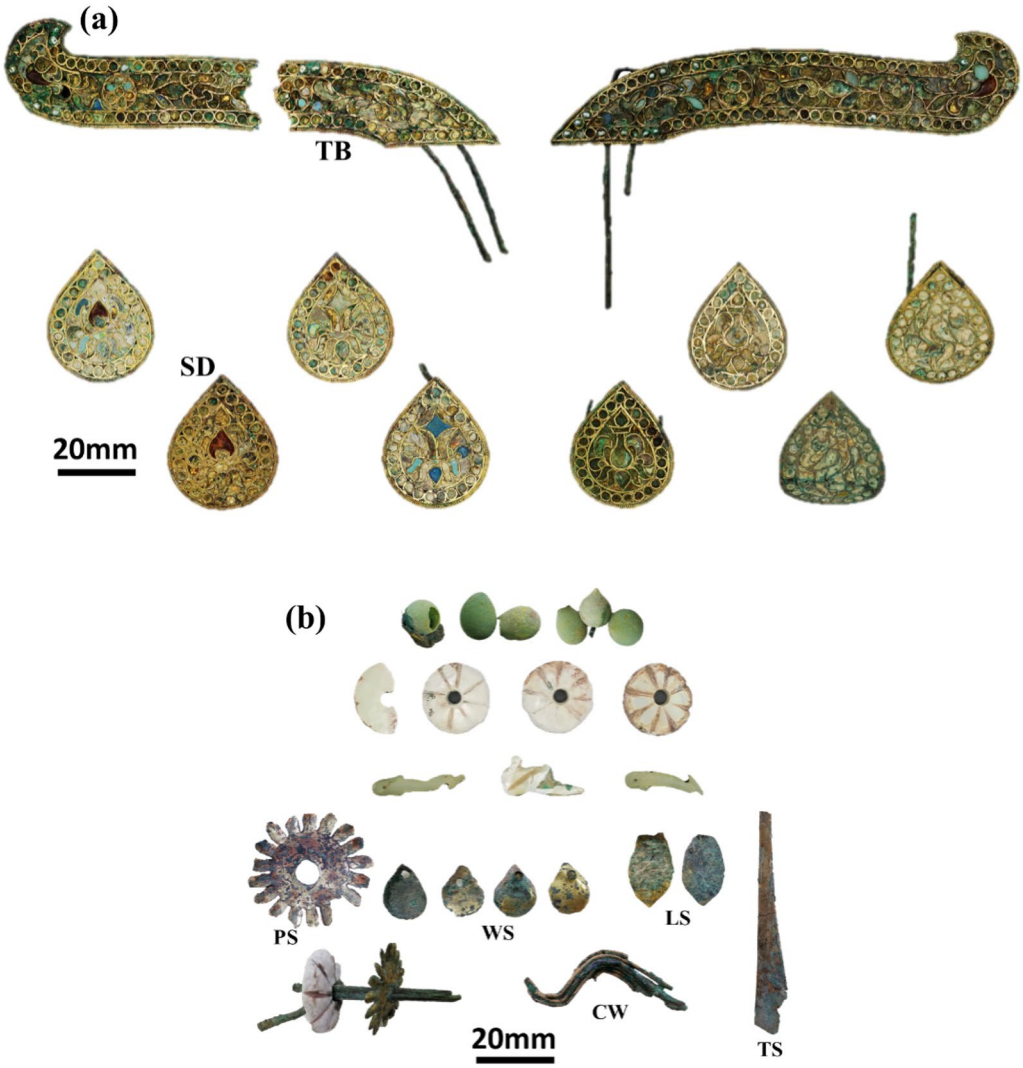

Fig. 2 **a** Temples and apricot-leaf ornaments of the ceremonial coronet [39]; and **b** some jade, mother-of-pearl, and metal components of the coronet

papers (300–1200 grit), and polished using a high-speed polishing machine (Buehler AutoMet 250) with a polishing agent (diameter: ~ 2.5 μm). The obtained cross-sectional samples with smooth surfaces were washed with ultra-pure water to remove the polishing agent and thoroughly dried. Herein, the Au-Cu system was taken as the research object to comprehensively analyze the copper-gilded products. Initially, the microstructure and composition of the surface and cross-section of the copper-gilded products were examined to gather relevant information. The heating temperature was inferred from the phase composition of the gold layer. Moreover, the distribution of Cu in the cross-section was evaluated to understand the impact of temperature on atomic diffusion. Subsequently, the heating temperature of the cultural relics was determined based on the phase composition of the gold layer and the diffusion behavior within the Au-Cu system. Through this comprehensive analysis, the formation mechanism and technological characteristics of copper gilding were elucidated.

Methods

Micromorphological and compositional analyses

The surface composition of the sample was nondestructively analyzed by X-ray fluorescence (XRF) spectrometry. Herein, the samples (TB, SD, PS, TS, LS, and WS) were mechanically cleaned to remove surface contaminants and then analyzed by XRF (EDAX Orbis, USA) using a rhodium target operating at 50 kV with an effective testing diameter of 5 mm. Notably, 3 – 5 analysis areas were selected for each sample, and each area was tested 3 – 5 times with a collection time of 150 s. The acquired data were screened and calculated to finally obtain the average compositional information of each sample surface.

The samples were examined and imaged with a ZEISS EVO MA 25 SEM microscope, equipped with an Oxford X-max 20 energy-dispersive X-ray spectrometer (EDS) console to obtain secondary electron (SEM) images, backscattered electron (BSE) images, and the alloy composition. SEM–EDS analysis was performed in line-avg mode with an accelerating voltage of 20 kV and an EDS working distance of approximately 8–9 mm. The ESD data were obtained by a standardless analysis method according to the Chinese national standard GB/T 17359–2012 [39]. An industrial copper standard sample was used for calibration and optimization. Each micro-area was analyzed at least three times, and the elemental results were averaged and normalized. After obtaining the micromorphology and compositional information of TB, SD, and the other samples by SEM–EDS, the damaged samples were cold inlaid and polished. The micromorphology, structure, and compositional information of the cross-sections of PS, TS, and the other samples were also analyzed.

Phase analysis

X-ray diffraction (XRD) patterns were used to identify metals and metallic compounds using an X-ray diffractometer (Kratos XRD-7000) equipped with a Cu Kα radiation source. The X-ray generator was equipped with a monochromator and a capillary attachment was used to enhance the signal intensity. The working state was controlled by the CPU. The 2θ range was from 10° to 90° and the scanning speed was 5°/min. The JADE 6.0 software package was used to compare each diffraction pattern with the reference patterns in the ICDD PDF2–2004 database.

The surface chemical features and bonding configurations of the samples were analyzed by X-ray photoelectron spectroscopy (XPS, Kratos, Axis Supra). CasaXPS software was used to fit the binding energy data and the Gauss-Lorentz method was used to fit the XPS spectra. To acquire the XPS spectra, an electron energy semi-spherical analyzer was fixed at a constant pass energy of 20 eV to ensure a constant energy resolution over the entire measured range. The energy resolution for the Ag $3d_{5/2}$ region after Ar^+ metal sputtering was 1.0 eV. The binding energy (BE) scale was calibrated by measuring the C 1 s signal (BE = 284.8 eV) of carbon [7]. The accuracy of the BE scale was ± 0.1 eV.

Results

Surface and cross-sectional micromorphology and elemental composition

The analysis conducted using surface XRF and cross-sectional EDS techniques revealed that the gold layer in all samples primarily consisted of Au, Hg, and Cu, as indicated in Table 1 and Table 2. The substrate was composed of pure Cu. The presence of Au and Hg as characteristic elements suggested the involvement of the mercury

Table 1 Surface chemical composition obtained by XRF

Sample	Composition (wt.%)[a]		
	Au	Hg	Cu
TB	70.4 ± 0.2	13.9 ± 0.2	15.7 ± 0.3
SD	63.5 ± 0.1	13.0 ± 0.2	23.5 ± 0.2
PS	36.1 ± 0.2	5.6 ± 0.1	58.3 ± 0.2
TS	36.2 ± 0.3	5.5 ± 0.1	58.3 ± 0.2
LS	40.2 ± 0.1	4.7 ± 0.2	55.0 ± 0.3
WS	40.0 ± 0.3	4.7 ± 0.2	55.4 ± 0.3

[a] The average value of multiple test results of multiple areas due to the non-uniformity of the surface composition

Table 2 Cross-sectional chemical composition determined using SEM–EDS

Sample			Composition (wt.%)[a]			
			Au	Hg	Ag	Cu
TB	Surface		87.4 ± 0.2	9.4 ± 0.1	1.3 ± 0.2	1.9 ± 0.3
	Cross-section	Gold layer	80.2 ± 0.2	9.7 ± 0.1	1.9 ± 0.1	8.2 ± 0.2
		Substrate [b]	–	–	–	100.0 ± 0.0
SD	Surface		86.6 ± 0.3	11.1 ± 0.2	1.4 ± 0.1	0.9 ± 0.1
PS	Surface		84.1 ± 0.3	8.8 ± 0.1	2.6 ± 0.1	4.5 ± 0.1
	Cross-section	Gold layer	78.3 ± 0.2	10.5 ± 0.1	1.5 ± 0.1	9.7 ± 0.2
		Substrate [b]	–	–	–	100.0 ± 0.0
TS	Surface		78.2 ± 0.3	8.6 ± 0.2	2.6 ± 0.1	10.6 ± 0.1
	Cross-section	Gold layer	77.1 ± 0.2	10.4 ± 0.3	1.8 ± 0.2	10.7 ± 0.1
		Substrate [b]	–	–	–	100.0 ± 0.2
LS	Surface		82.7 ± 0.3	8.9 ± 0.2	1.7 ± 0.1	6.8 ± 0.2
	Cross-section	Gold layer	70.7 ± 0.2	7.6 ± 0.1	–	21.8 ± 0.1
		Substrate [b]	–	–	–	100.0
WS	Surface		85.8 ± 0.1	7.2 ± 0.3	2.2 ± 0.1	4.8 ± 0.2
	Cross-section	Gold layer	66.4 ± 0.1	5.3 ± 0.1	2.9 ± 0.2	25.4 ± 0.1
		Substrate [b]	–	–	–	100.0
CW	Surface		87.3 ± 0.3	7.9 ± 0.1	3.3 ± 0.1	1.5 ± 0.1
	Cross-section	Gold layer	72.7 ± 0.1	12.2 ± 0.2	2.8 ± 0.1	12.3 ± 0.2
		Substrate [b]	–	–	–	100.0

[a] The average value of multiple test results of multiple areas

[b] The uncorroded areas

gilding process [43]. This led to the speculation that the coronet decoration components were made of gilding copper. The gold layer was found to be a combination of gold and various gold amalgams, resulting in variations in the Hg content across different samples, as presented in Table 1. Additionally, the Cu content on the surface was significantly higher compared to that in the cross-section. This showed that the corrosion products formed by the diffusion of substrate Cu were concentrated on the surface of the gold layer. The variation of the Cu content within the cross-section of the gold layer followed the diffusion law associated with corrosion, as indicated in Table 2 [44, 45].

The BSD images of the golden surface in the sample (Figs. 3a, d, e, g) revealed the presence of flat and compact areas exhibiting distinct and consistent scratches aligned in a specific direction. These observations provide strong evidence that the relatively flat and smooth gold surface of the gilded products was indeed attained through the polishing process. In other areas of the samples, a significant number of fine gold particles, approximately 2 μm in diameter, were observed to cluster together (Fig. 4a, b, e, a, e, g). These particles exhibit a characteristic granular morphology commonly associated with mercury gilding products, and their presence is noticeable even on the unpolished surface. Furthermore, in the cross-sectional BSD images, the gold layers in all samples were easily discernible and relatively thin, measuring approximately 4–6 μm in thickness (Fig. 3c, b, d, f, h). In contrast to the smooth and compact surface, the cross-section of the gold layer exhibited an accumulation of granules with numerous pores interspersed between them. This distinctive cross-sectional structure arose from the formation of gas channels and granules within the gold layer during the heating process, as a result of mercury evaporation. Notably, these unique features of the gilded products remained intact even after surface polishing. The higher-magnification cross-sectional images revealed several small holes in the interface between the gold layer and substrate (Fig. 5a, b). The EDS results of different areas showed that the area A of the substrate only contained Cu, while the area B contained a significant amount of O and Cl in addition to Cu. In the gold layer, area C adjacent to the substrate contained 48.3 wt.% Cu, 44.1 wt.% Au, and 6.5 wt.% Hg. Surface area D of the gold layer had significantly higher Au and Hg content, while the content of Cu sharply decreased to 5.2 wt.% (Fig. 5a and Table 3). The same component distribution was also reflected in the EDS results of areas E and F (Fig. 5b and Table 3). The gold layer consisted of an uneven mixture of gold, mercury, and various gold amalgams. Thus, in different samples or different areas of the

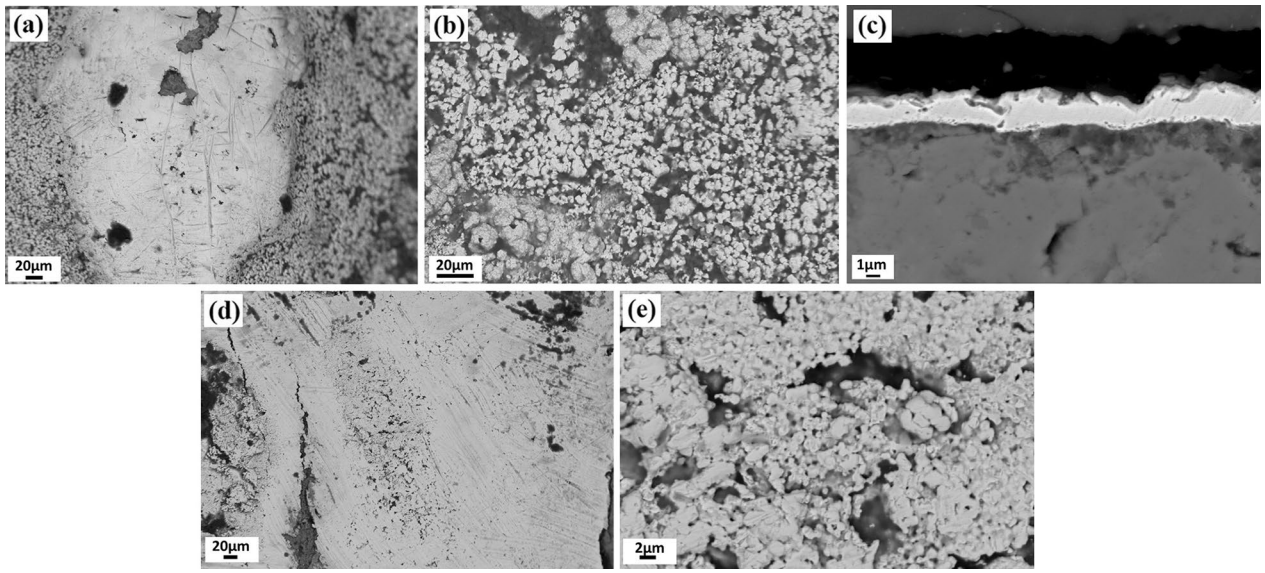

Fig. 3 **a** Flat surface and scratch of TB; **b** Granular morphology of the gold layer of TB; **c** Cross-sectional BSE-SEM image of TB; **d** Polishing traces on the surface of SD; and **e** Granular morphology of the gold layer of SD

same sample, the mercury content was different ((Table 3 D, F). Due to the long-term copper corrosion and diffusion in these cultural relics, the copper content was relatively high and the mercury content was low in some areas of the cross-section of the gold layer, resulting in a significant deviation in mercury content (Table 3, areas C, E). Plotting the cross-sectional Cu content with depth showed that the substrate contained the highest amount of Cu, and the Cu content gradually decreased toward the gold layer. Overall, the Cu content remained above 20 wt.% within 1 μm of the interface. However, when this distance exceeded 2 μm, the Cu content dropped below 8 wt.% (Fig. 6a, b).

As a consequence of prolonged exposure to the burial environment, the substrate underwent gradual corrosion [46], leading to the formation of dark gray areas comprising copper oxides, chlorides, and other corrosion by-products. However, Cu atoms diffused from the substrate towards the gold layer, with a substantial number of copper atoms diffusing within a distance of only 2 μm from the interface. This phenomenon can be attributed to the influence of the diffusion driving force.

The samples were selected with an appropriate size and relatively flat surface for XRD analysis, as reported in Fig. 7. The diffraction peaks at $2\theta = 30.8°$, 42.0°, 64.3°, and 73.1° corresponded to the characteristic peaks of the gold-copper phase Au_3Cu (PDF #34–1302) [47]. However, some characteristic peaks overlapped with those of Au (PDF # 04–0784) at $2\theta = 38.2°$, 44.4°, 64.6°, 77.5°, and 81.7° and a Cu_2O (PDF # 05–0667) copper oxide peak at $2\theta = 42.3°$. XPS was applied to characterize the surface composition and oxidation state of Au_3Cu in detail (Fig. 8). After peak fitting and C 1 s correction, for the Cu 2p spectrum, the two peaks at 931.2 eV and 950.8 eV in the Cu 2p spectrum were assigned to the Cu $2p_{3/2}$ and Cu $2p_{1/2}$ orbits of metallic Cu (Fig. 8b) [48]. Moreover, the Cu peaks at 933.1 eV and 952.7 eV and the O1s pecks at 530.3 eV were assigned to Cu_2O species (Fig. 8b, d). The peaks at 934.4 eV and 954.0 eV were ascribed to Cu^{2+} species. The Au 4f spectrum exhibited $4f_{7/2}$ and $4f_{5/2}$ pecks at binding energies (B.E.) of 84.7 eV and 88.8 eV, respectively (Fig. 8c). The peaks at 99.9 eV and 103.9 eV coincided with the metallic state Hg (Fig. 8e). Compared with metallic state, the band positions of Au 4f spectrum were slightly shifted toward higher binding energies. Correspondingly, the B.E. values of $Cu2p_{3/2}$ and $Cu2p_{1/2}$ shifted in the opposite direction, while the Hg4f band positions remined unchanged. This can be attributed to the electronic interaction between Au and Cu in the alloy [49]. It is reasonable to infer that the transfer of valence electrons transfer from the Cu atom to the Au atom is caused by their discrepancy of electronic negativities, resulting in the redistribution of interatomic charges [50]. Therefore, during the heating process of the gold amalgam and substrate, a new Au-Cu phase was formed by the redistribution of interatomic charges in the system.

Mercury was detected in the gold layer by EDS, but the characteristic peaks of gold-mercury compounds were not observed by XRD. One reason might be that the size of the detection area was too small and the compounds were not evenly distributed in the gold layer.

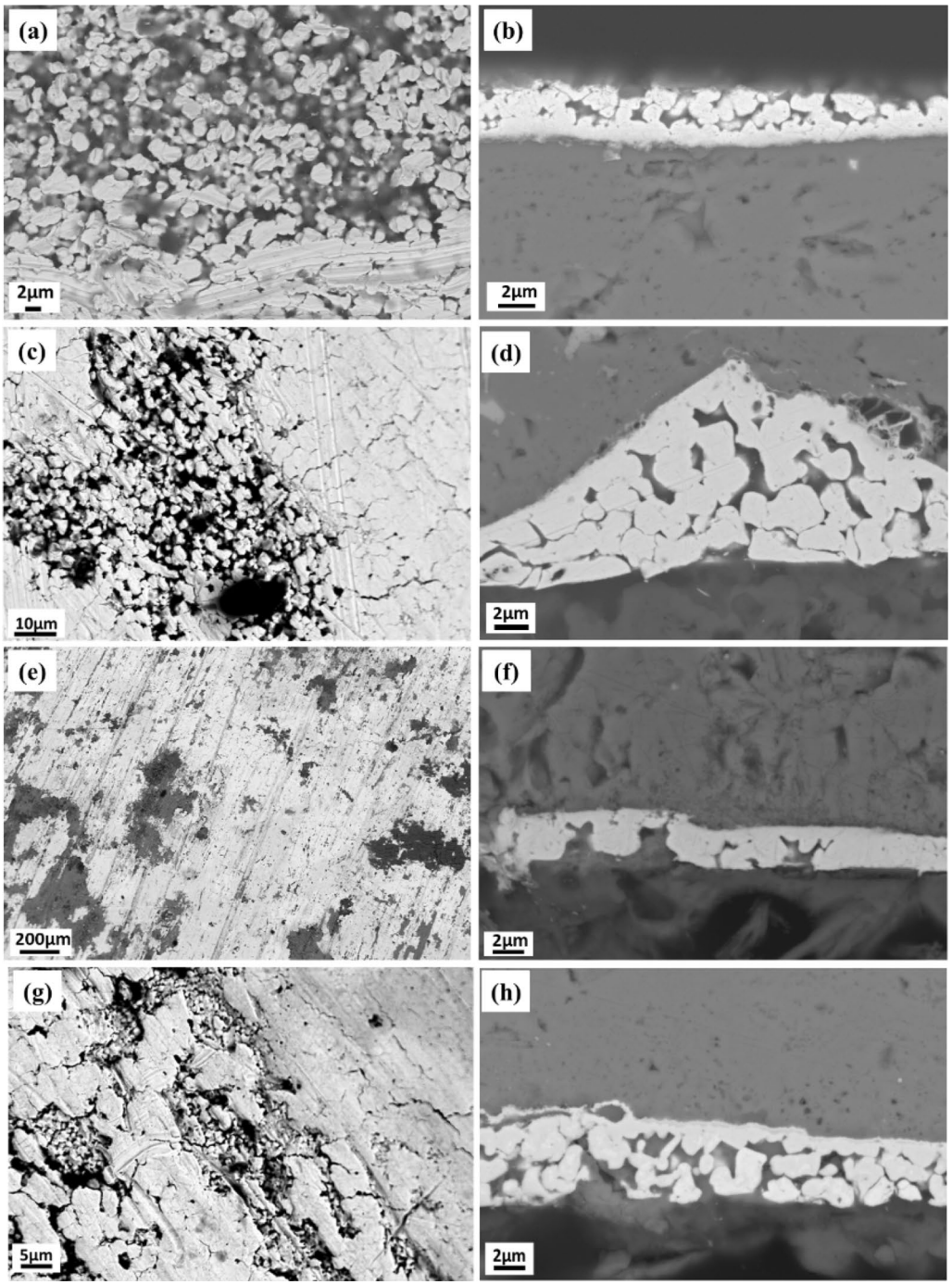

Fig. 4 Granular morphology of the surface and cross-sectional areas of PS **a**, **b**; TS **c**, **d**; LS **e**, **f**; and LS **g**, **h**

Thus, gold-mercury compounds were not found in the effective area. Another potential reason was that stable gold-mercury compounds were not formed at the heating temperature of the gilding process [19]. In addition, although Cu was not the main component of the gold layer (less than 10 wt.%), the characteristic peaks of gold-copper compounds and copper oxide minerals were still detected by XRD because the X-ray penetration depth for different elements generally reaches tens of microns [51]. These characteristic peaks were due to the phase

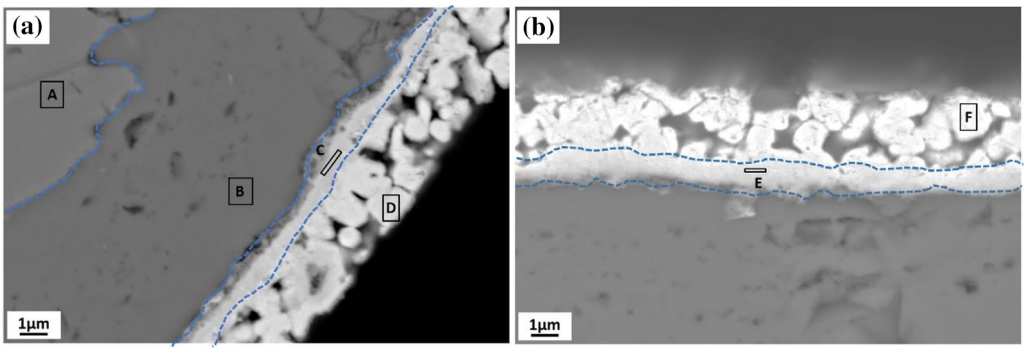

Fig. 5 Different areas on the cross-section of CW **a** and PS **b**

Table 3 Cross-sectional chemical composition of CW and PS determined using SEM–EDS

Analysis area	Composition (wt.%)[a]					
	Au	Hg	Ag	Cu	O	Cl
A	–	–	–	100.0	–	–
B	–	–	–	59.0 ± 0.3	22.8 ± 0.3	18.3 ± 0.2
C	44.1 ± 0.2	6.5 ± 0.1	1.1 ± 0.2	48.3 ± 0.2	–	–
D	76.4 ± 0.3	16.1 ± 0.2	2.3 ± 0.1	5.2 ± 0.1	–	–
E	32.2 ± 0.2	3.0 ± 0.2	–	65.8 ± 0.1	–	–
F	77.3 ± 0.3	12.3 ± 0.2	2.2 ± 0.1	8.2 ± 0.1	–	–

[a] The average value of multiple test results of different areas

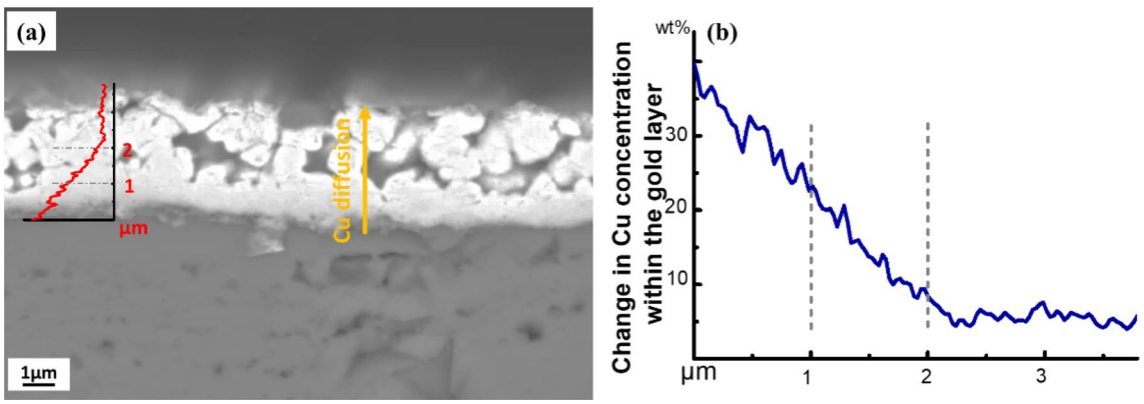

Fig. 6 **a** Cross-sectional BSE image of PS and **b** change in Cu concentration within the gold layer

inside the gold layer or even the substrate. The copper oxide was undoubtedly formed by the diffusion of copper from the substrate and the slow reaction of this copper with environmental oxygen during the long-term burial of the cultural relics [43]. However, the formation of gold-copper compounds in the gilding process required an appropriate temperature and potentially other harsh conditions [52].

Discussion

The investigation into gilding processes has initially relied on ancient literature records and has gradually been substantiated through the analysis of cultural relics. It is evident that the gold layers of gilded products are formed through the heating of gold amalgam. However, there has been ongoing debate regarding the specific formation mechanism of these layers. Among the

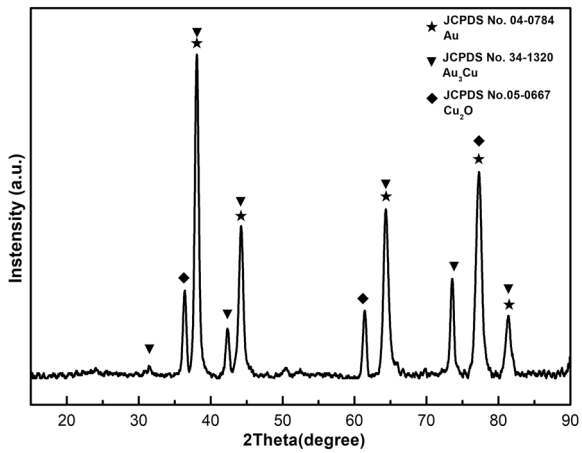

Fig. 7 XRD patterns of the PS

various factors influencing the analysis of the gilding process, the heating temperature has garnered particular attention. Understanding the heating temperature is crucial in unraveling the formation mechanism of gilding. In the case of copper gilding, most of the mercury evaporates and exits the system during the heating process, while any residual traces of mercury at the interface exhibit minimal interaction with copper. Consequently, previous research suggests that studying the interface between the gold layer and the substrate should primarily focus on the Au-Cu system. Building upon this premise, the present work analyzes the formation mechanism of the copper gilding process and explores the interaction between the gold layer and the substrate.

Phase composition and formation mechanism of the gold layer

The phase composition of an Au-Cu system is related to its processing temperature. Therefore, the heating temperature in the gilding process was preliminarily defined by analyzing the Au-Cu intermetallic compound in the gold layer.

Cu and Au possess the same valence state with a small difference in electronegativity. Therefore, the solute atoms only substitute the solvent atoms in the crystal lattice without structural changes during interdiffusion at low temperatures [53]. The diffusion of Cu into Au under the influence of heat only results in a random distribution of Cu atoms in the FCC-structured Au, and there is no atomically ordered arrangement in the crystal lattice. However, when the system reaches a certain temperature range, the Cu and Au atoms gradually form a new ordered arrangement. At this time, the ordered solid solution on the Cu-Au interface forms new phases (i.e., Cu-Au intermetallic compounds such as $AuCu_3$, Au_3Cu, and AuCu) (Fig. 9) [54]. The Au-Cu phase diagram shows that

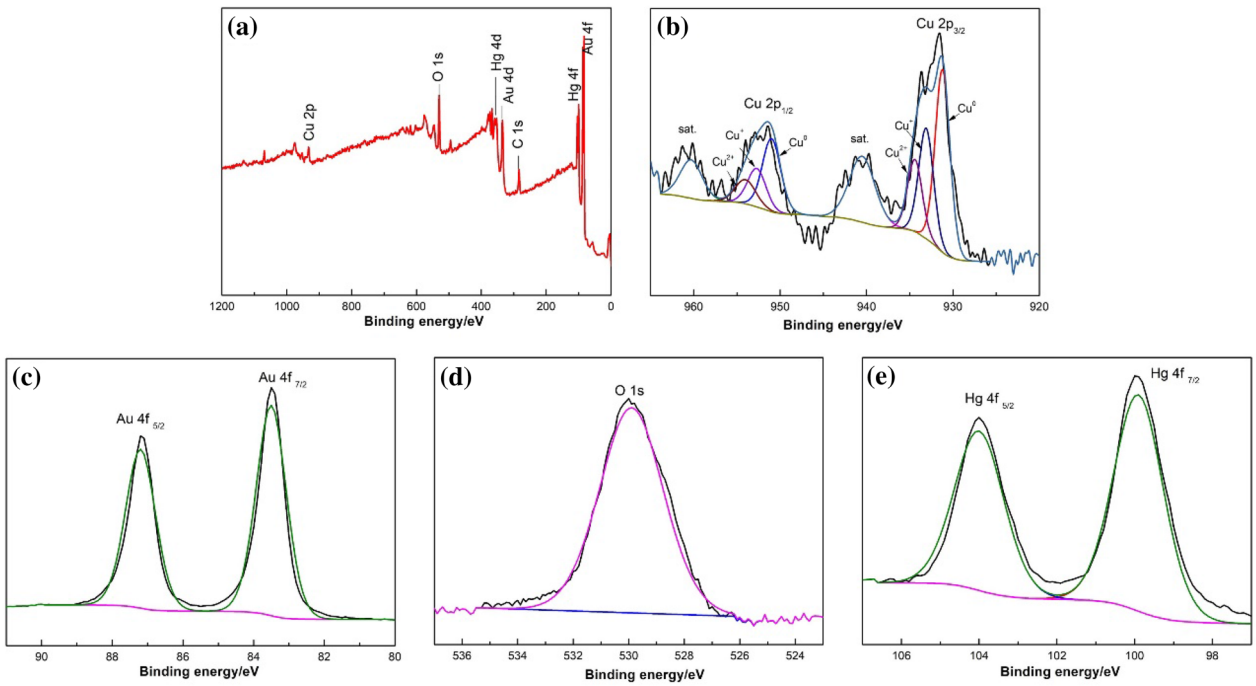

Fig. 8 XPS spectra of PS: **a** survey, **b** Cu 2p, **c** Au 4f, **d** O 1 s, and **e** Hg 4f spectra

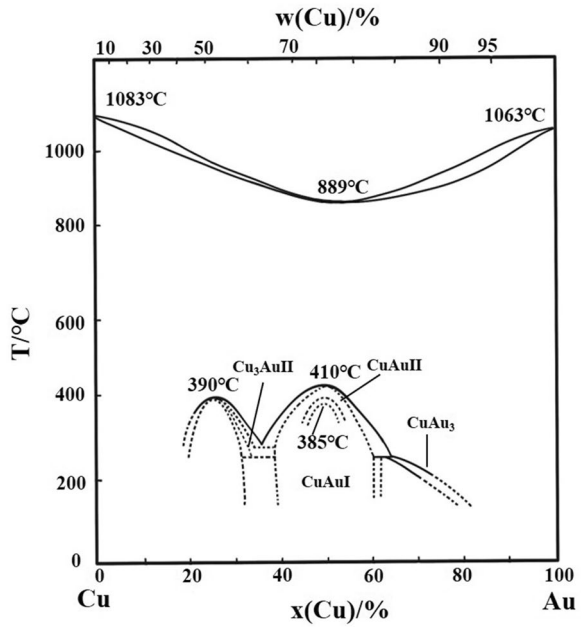

Fig. 9 Au-Cu phase diagram (Reprinted with permission from Ref. [54])

stable intermetallic compounds cannot be formed at temperatures below 150 ℃ or above 410 ℃ [55]. The solid–liquid transition of the same composition occurs between (Cu, Au) and AuCuII at 410 ℃ and between (Au, Cu) and $AuCu_3I$ at 390 ℃. The transition temperature between AuCu II and AuCuI is 385 ℃. The transition between (AuCu) and AuCu II + $AuCu_3I$ occurs at 285 ℃. At 240 ℃, Au_3Cu is formed by a peritectic reaction. In previous studies, $AuCu_3$ and AuCu have been observed on the gold layers of some gold-plated copper samples that were treated at 250 ℃ and 300 ℃ [56]. Therefore, the existence of Au-Cu compounds proved that the gold layer of the cultural relics studied in this work was indeed formed by heating. This can be considered as one of the technical features of the gilding process. Moreover, because Au_3Cu was found on the gold layer, the gilding heating temperature of the gilded coronet was speculated to be 240–285 ℃ according to the Au-Cu phase diagram. The gold amalgam in the gilding was a mixture of Au, Hg, and various Au-Hg intermetallic compounds. Mercury slowly evaporates when the temperature exceeds 8 ℃, and the evaporation rate increases with increasing temperature [57]. Therefore, at 240–285 ℃, excess mercury left the system. In addition, because the Au-Hg system was a special open system during heating, Au-Hg compounds began to experience phase transformation when the temperature exceeded room temperature. For example, when the temperature exceeded 122 ℃, the gray γ-Au_2Hg in the gold amalgam began to transform into golden Au_3Hg. As the temperature gradually increased, new phase transition reactions continued to occur in the system [58]. Therefore, the formation mechanism of the gold layer of this copper gilt product can be described as follows: the paste-like gold amalgam was transformed into solid gold mercury compounds through a solid-state reaction at low temperatures.

Bonding mechanism of gold layer and substrate—atomic diffusion during gilding process

A large number of mercury atoms in the gold amalgam rapidly evaporated during the heating process, generating a large number of gas channels and causing the gold layer to exhibit a fine particle morphology. Moreover, the Au-Cu binary system was left at the interface. The morphological characteristics and gas channels of the gold layer provided defect-containing diffusion channels for Cu atoms [45]. Therefore, the relationship between Cu diffusion and the heating temperature provided useful insights into the heating-assisted gilding process.

There are two possible diffusion mechanisms of the Au-Cu system [59]. Classical bulk diffusion, also known as lattice diffusion, involves vacancy-assisted atomic exchange, where the reaction is completed in a reasonable time if the temperature is near the melting point. Rapid diffusion can occur along defect paths even at low temperatures in different systems. One should note that defects such as grain boundaries and dislocations are common in metals and act as rapid transportation channels through metallic layers, favoring the rapid diffusion mechanism [59, 60]. The porous structure of the gold layer of the gilding products indicated that the diffusion of substrate elements likely occurred via the defect-assisted diffusion mechanism. Moreover, for the copper gilded crown, the heating temperature (240–285 ℃) was less than half of the melting point. Thus, copper atoms rapidly diffused to the gold layer along the defects and the diffusion mechanism of the copper atoms was clearly rapid diffusion. In addition, the formation of new Au-Cu phase layers is inevitable when the Au-Cu system undergoes diffusion at a certain temperature, which has been shown in many previous studies [60, 61]. Whether in the Au-Cu phase or Au phase, the diffusion mode of copper is rapid diffusion along defects (grain boundaries, etc.) at temperatures below half the melting point [54].

Furthermore, it is important to highlight that during the prolonged storage of copper-gilt products, the atoms from the substrate undergo slow diffusion towards the gold layer driven by corrosion at room temperature. The diffusion of copper, as depicted in Fig. 6, was predominantly associated with the corrosive processes experienced by these gilding artifacts while being buried for an extended period. The bimetallic

structure of these artifacts accelerated the corrosion of copper, facilitated by the migration of Cu^{+} and Cu^{2+} ions through micropores and microchannels within the gilding layer. Hence, two sources of copper atoms within the gold layer were identified: those resulting from defect-assisted diffusion during the heating process and those arising from the long-term diffusion of the substrate due to corrosion at room temperature [61].

During the heating process, defect-assisted diffusion played a significant role in the formation of gilded crowns. Copper atoms, driven by heat, undergone diffusion into the gold layer, leading to the inevitable creation of a new layer known as Au_3Cu phase, in conjunction with the gold. According to the formation conditions of Au_3Cu, this phase was clearly a product of heating in the gilding process. Significantly, the copper atoms present in Au_3Cu originated solely from rapid diffusion during heating and were unrelated to corrosion diffusion during preservation. Moreover, the newly formed Au_3Cu intermetallic compound was close to the substrate side due to Cu enrichment [61, 62]. The distribution of Cu in the cross-section of the gilded product was also analyzed (Fig. 6b). Cu atoms diffused outward from the interface between the substrate and the gold layer. A linear downward trend in the Cu concentration was observed within 2 μm of the interface. Above 2 μm, the Cu concentration gradually stabilized. It was speculated that the rapid diffusion of Cu during heating did not exceed a distance of 2 μm. Moreover, the content of Cu in the area within 1 μm away from the substrate was 23−39 wt.%, which was much higher than that of Au_3Cu (9.77 wt.%). Further than 2 μm from the substrate, the Cu content was only 5–7 wt.%, which was significantly lower than the content of Au_3Cu (Fig. 6a, b and Table 4). Obviously, the thickness of Au_3Cu phase would not exceed 2 μm. Thus, the diffusion distance of Cu during the heating would not exceed 2 μm.

In the heating process of copper gilding crowns, copper exhibited rapid diffusion along the defects present in the gold layer, resulting in the formation of a diffusion layer that was typically no more than 2 μm in thickness. Furthermore, the bonding between the gold layer and the substrate occurred through the diffusion of copper atoms during the heating process.

Table 4 Cu concentration at different diffusion distances

Diffusion distance/μm[a]	Cu content (wt.%) [b]
0	100.0
~1	23–39
>2	5–7

[a] Along the copper diffusion direction in Fig. 6

[b] Concentration range obtained after multi-point measurements

Relationship between diffusion and temperature in the Au-Cu system

The temperature plays a crucial role in determining the mechanism and pathway of solid-phase diffusion in binary systems [63]. It significantly influences the diffusion coefficient and rate, thereby shaping the process of diffusion in such systems [64]. The temperature dependence of diffusion coefficient D is related to temperature according to the following equation:

$$D = D_0 \exp\left(-\frac{Q_d}{RT}\right)$$

where D_0 is a temperature-independent coefficient, Q_d is the activation energy of diffusion, R is the gas constant, and T is the absolute temperature. In the Au-Cu system, the diffusion rate of copper atoms along defects is much faster than that of gold atoms. To establish the diffusion model, it can therefore be assumed that the gold atoms do not diffuse [63, 64]. For the copper-gilded crown, the diffusion mechanism of Cu during the heating process was rapid diffusion. The D' (defect path diffusion coefficient) value was an order of magnitude greater than D (lattice diffusion constant) [65]. Thus, D' was more suitable for calculations.

In diffusion calculations, Fick's second law can comprehensively describe non-stationary diffusion processes where concentration changes over time. The general diffusion coefficient is a constant. The boundary conditions of Fick's second law are: (1) the concentration of diffusing substance C_s remains constant throughout the entire diffusion process; (2) a certain amount of the diffusing substance diffuses from the surface to the interior. During the gilding process of the cultural relics studied in this work, copper atoms rapidly diffused along the defects of the gold layer during heating [65]. The Cu substrate provided an unlimited supply of Cu atoms to the gold layer, maintaining a constant surface concentration (C_s) at all times. Therefore, the relationship between diffusion distance and concentration can be solved using Fick's second law. In non-stationary diffusion processes, the change in the concentration over time at a distance of x is equal to the negative value of the change in the diffusion flux with distance [66]. If D' is independent of concentration, the penetration of diffusing species in an infinite system can be described by this relationship [62, 67]:

$$\frac{C_x - C_0}{Cs - C_0} = 1 - erf\left[x \Big/ 2\sqrt{D't}\right]$$

Table 5 Values of error function erf(x). [a] erfc(x) = 1-erf(x)

x	erf(x)	erfc(x)
0.00	0.000000000000	0.000000000000
….		
1.16	0.899096168851	0.100903831149
1.17	0.902000369835	0.097999630165
1.18	0.904837401978	0.095162598022
….		

[a] Selected data. The complete data is in the Table 6

where C_x (wt.%) refers to the concentration of diffusing species (Cu) at penetration distance *x* (cm) and time t (s), C_s corresponds to the constant surface concentration, and C_0 denotes the original concentration of Cu in the solid. The error function erf $(x/2\ (Dt))^{1/2}$ is a tabulated function (Tables 5, 6). D (cm^2/s) refers to the diffusion coefficient of the diffusing species, and substituting D' here is more appropriate, as explained above. Furthermore, in the copper gilding process, copper diffusion occurs primarily along grain boundaries and other defects at temperatures below half the melting point, regardless of whether it's in Au-Cu or Au phases [61]. The rate of copper diffusion is rapid, and the distance traveled depends on factors such as the diffusion coefficient (D') and time [64]. Moreover, recent research have shown that D' of copper in Au or Au-Cu system falls within the range of 10^{-12} at temperatures ranging from 200 °C to 350 °C. Therefore, using an appropriate diffusion coefficient enables us to obtain a reliable estimation of the diffusion distance. For instance, in a Cu-Au system, the defect-assisted diffusion coefficient of copper atoms along grain boundaries at a temperature of 320 °C is estimated to be approximately 1×10^{-12} cm^2/s [60] or $2–3.5\times10^{-12})$ cm^2/s [68]. Furthermore, at a temperature of 300 °C, the reported diffusion coefficient of copper in an Au_3Cu alloy is approximately 2.6×10^{-12} cm^2/s [61]. In the manuscript, we have utilized a value of $1–3.5\times10^{-12}$ cm^2/s for calculations, encompassing all available data.

In addition, achieving the desired thickness of the gold layer may indeed require repeated coating and heating processes. However, based on previous reports and our simulation experiments, the diffusion mode and distance of copper are not affected by these repeated heating processes. In the actual fire gilding process, the heating time is correlated with the thickness of the gold layer, but each individual heating process is relatively short [10]. For instance, it takes less than 10 min of heating to obtain a gold layer with a thickness of 5–10 μm, and less than 2 min for a 2 μm gold film [3]. Significantly, in the diffusion process of the Au-Cu system, adhering to the boundary condition $(L > 4.6(Dt)^{1/2})$, even a gold layer with a minimum thickness of 2 μm can be considered as an infinite diffusion system. Additionally, when taking into account the heating time and diffusion coefficient during the formation of a 2 μm thick gold layer, it has been determined that less than 1wt.% of copper atoms can diffuse to a distance of 0.7 μm, while less than 7wt.% of copper atoms can diffuse to a distance of 0.5 μm. As a result, during the second coating, the concentration at the interface between the gold layer and the substrate can still be simplified to 100wt.% for calculation purposes. In the approximation of the copper gilding process as an ideal model calculation, the diffusion coefficient is dependent on the cumulative heating time rather than the number of heating cycles applied. At this stage, the heating time represents the cumulative heating time of both coating cycles, and the thickness of the gold layer corresponds to the total thickness from both cycles.

Typically, it is widely accepted that heating a copper substrate for a duration of 10–15 min is adequate to achieve a high-quality golden film when gilding [22]. The gold layer thickness of all the gilded ornaments was measured to be 4–6 μm. Thus, at t = 900 s (Choose the longest possible time), the value of $4.6(Dt)^{1/2}$ was 1.4–2.6 μm, conforming to the assumption of $L > 4.6(Dt)^{1/2}$. It was assumed that the original concentration of Cu in the gold layer was $C_0 = 0$, and the concentration in the substrate was $C_s = 100$ wt.%, For heating time t = 15 min = 900 s and $C_x = 9.77$ wt.% (Cu in Au_3Cu), x = 0.7–1.3 μm. Therefore, the Cu atoms diffused by 0.7–1.3 μm into the gold layer during heating. This analysis is consistent with the measured thickness of the Au_3Cu layer in the cross-section images (< 2 μm).

Therefore, the calculation process of Cu defect diffusion in the Cu-Au system provided additional confirmation that copper coronets were gilded at temperatures ranging from 240 to 285 ℃ for approximately 15 min. This gilding process resulted in the formation of a Cu diffusion layer at the interface between the gold layer and the substrate, with a maximum thickness of 2 μm. The diffusion layer was crucial as it facilitated the firm adhesion of the gold layer to the substrate, achieved through defect-assisted diffusion at lower temperatures [68, 69].

Conclusions

In this study, a comprehensive analysis of a copper-gilded coronet from the *Sui* or *Tang* dynasties was conducted using XRF, SEM–EDS, XRD, and XPS techniques to investigate its surface and cross-sectional micromorphology, structure, and composition. The presence of mercury and the granular morphology of the gold layer were distinct characteristics observed in the gilding products. Additionally, one of the main phases identified in the gold layer was Au_3Cu. Considering the position of Au_3Cu in the Au-Cu phase diagram, it was estimated that the heating

Table 6 Values of the error function erf(x)

Error function	$\mathbf{erf(x)} = \frac{2}{\sqrt{\pi}} \int_0^x \exp(-y^2)dy$
erfc(x) = 1-erf(x)	

X	erf(x)	erfc(x)	X	erf(x)	erfc(x)	X	erf(x)	erfc(x)
0.00	0.000000000000	1.000000000000	0.37	0.399205982861	0.600794017139	0.74	0.704677825150	0.295322174850
0.01	0.011283415555	0.988716584445	0.38	0.409009451768	0.590990548232	0.75	0.711155429840	0.288844570160
0.02	0.022564574690	0.977435425310	0.39	0.418738697780	0.581261302220	0.76	0.717536534054	0.282463465946
0.03	0.033841222338	0.966158777662	0.40	0.428392351896	0.571607648104	0.77	0.723821436877	0.276178563123
0.04	0.045111106142	0.954888893858	0.41	0.437969090031	0.562030909969	0.78	0.730010238060	0.269989761940
0.05	0.056371977793	0.943628022207	0.42	0.447467618261	0.552532381739	0.79	0.736103240130	0.263896759870
0.06	0.067621594389	0.932378405611	0.43	0.456886694328	0.543113305672	0.80	0.742100790385	0.257899209615
0.07	0.078857719765	0.921142280235	0.44	0.466225114978	0.533774885022	0.81	0.748003138393	0.251996861607
0.08	0.090078125833	0.909921874167	0.45	0.475481719382	0.524518280618	0.82	0.753810590156	0.246189409844
0.09	0.101280593901	0.898719406099	0.46	0.484655389454	0.515344610546	0.83	0.759523625314	0.240476374686
0.10	0.112462915992	0.887537084008	0.47	0.493745050147	0.506254949853	0.84	0.765142559892	0.234857440108
0.11	0.123622896147	0.876377103853	0.48	0.502749669700	0.497250330300	0.85	0.770667932983	0.229332067017
0.12	0.134758351714	0.865241648286	0.49	0.511668259856	0.488331740144	0.86	0.776100121993	0.223899878007
0.13	0.145867114826	0.854132885174	0.50	0.520499876035	0.479500123965	0.87	0.781439724674	0.218560275326
0.14	0.156947033051	0.843052966949	0.51	0.529243617480	0.470756382520	0.88	0.786687219425	0.213312780575
0.15	0.167995971414	0.832004028586	0.52	0.537898627358	0.462101372642	0.89	0.791843126770	0.208156873230
0.16	0.179011813181	0.820988186819	0.53	0.546464092831	0.453535907169	0.90	0.796908112895	0.203091887105
0.17	0.189992461178	0.810007538822	0.54	0.554939245085	0.445060754915	0.91	0.801882743251	0.198117256749
0.18	0.200935838984	0.799064161016	0.55	0.563323359330	0.436676640670	0.92	0.806767619642	0.193232380358
0.19	0.211839892105	0.788160107895	0.56	0.571615763455	0.428384236545	0.93	0.811563473736	0.188436526264
0.20	0.222702589127	0.777297410873	0.57	0.579815805683	0.420184194317	0.94	0.816270948330	0.183729051670
0.21	0.233521922850	0.766478077150	0.58	0.587922899753	0.412077100247	0.95	0.820890717620	0.179109282380
0.22	0.244295911388	0.755704088612	0.59	0.595936496378	0.404063503622	0.96	0.825423574670	0.174576425330
0.23	0.255022599259	0.744977400741	0.60	0.603856089780	0.396143910220	0.97	0.829870230340	0.170129769660
0.24	0.265700058433	0.734299941567	0.61	0.611681217488	0.388318782512	0.98	0.834231422458	0.165768577542
0.25	0.276326389365	0.723673610635	0.62	0.619411460101	0.380588539899	0.99	0.838508000774	0.161491999226
0.26	0.286899723185	0.713100276815	0.63	0.627046441016	0.372953558984	1.00	0.842700735175	0.157299264825
0.27	0.297418218507	0.702581781493	0.64	0.634585826132	0.365414173868	1.01	0.846810447700	0.153189552300
0.28	0.307880067977	0.692119932023	0.65	0.642029323520	0.357970676480	1.02	0.850837952060	0.149162047940
0.29	0.318283495789	0.681716504211	0.66	0.649376683060	0.350623316940	1.03	0.854784156064	0.145215843936
0.30	0.328626759359	0.671373240641	0.67	0.656627696054	0.343372303946	1.04	0.858649899788	0.141350100212
0.31	0.338908150169	0.661091849831	0.68	0.663782194814	0.336217805186	1.05	0.862436066652	0.137563933348
0.32	0.349125994593	0.650874005407	0.69	0.670840052208	0.329159947792	1.06	0.866143531268	0.133856468732
0.33	0.359278654683	0.640721345317	0.70	0.677801193147	0.322198806853	1.07	0.869773250224	0.130226749776
0.34	0.369364528928	0.630635471072	0.71	0.684665263995	0.315334736005	1.08	0.873326118594	0.126673881406
0.35	0.379382052969	0.620617947031	0.72	0.691432825427	0.308567174573	1.09	0.876803068202	0.123196931798
0.36	0.389329700289	0.610670299711	0.73	0.698103703680	0.301896296320	1.10	0.880205040976	0.119794959024
1.11	0.883532970435	0.116467029565	1.52	0.968413493245	0.031586506755	1.93	0.993655649566	0.006344350434
1.12	0.886787854405	0.113212145595	1.53	0.969516205881	0.030483794119	1.94	0.993922570352	0.006077429648
1.13	0.889970639901	0.110029360099	1.54	0.970585687054	0.029414312946	1.95	0.994179333115	0.005820666885
1.14	0.893082301682	0.106917698318	1.55	0.971622730809	0.028377269191	1.96	0.994426275041	0.005573724959
1.15	0.896123820836	0.103876179164	1.56	0.972628119883	0.027371880117	1.97	0.994663724270	0.005336275730
1.16	0.899096168851	0.100903831149	1.57	0.973602625589	0.026397374411	1.98	0.994892000052	0.005107999948
1.17	0.902000369835	0.097999630165	1.58	0.974547007706	0.025452992294	1.99	0.995111412902	0.004888587098

Table 6 (continued)

Error function	$\mathbf{erf(x) = \frac{2}{\sqrt{\pi}} \int_0^x \exp(-y^2) dy}$

erfc(x) = 1-erf(x)

X	erf(x)	erfc(x)	X	erf(x)	erfc(x)	X	erf(x)	erfc(x)
1.18	0.904837401978	0.095162598022	1.59	0.975462011997	0.024537988003	2.00	0.995322264755	0.004677735245
1.19	0.907608264626	0.092391735374	1.60	0.976348379983	0.023651620017	2.01	0.995524849121	0.004475150879
1.20	0.910313959958	0.089686040042	1.61	0.977206833628	0.022793166372	2.02	0.995719451244	0.004280548756
1.21	0.912955492333	0.087044507667	1.62	0.978038085776	0.021961914224	2.03	0.995906348259	0.004093651741
1.22	0.915533855545	0.084466144455	1.63	0.978842837391	0.021157162609	2.04	0.996085809348	0.003914190652
1.23	0.918050082203	0.081949917797	1.64	0.979621777518	0.020378222482	2.05	0.996258095898	0.003741904102
1.24	0.920505165437	0.079494834563	1.65	0.980375583261	0.019624416739	2.06	0.996423461660	0.003576538340
1.25	0.922900112029	0.077099887971	1.66	0.981104919763	0.018895080237	2.07	0.996582152902	0.003417847099
1.26	0.925235927850	0.074764072150	1.67	0.981810440204	0.018189559796	2.08	0.996734408567	0.003265591433
1.27	0.927513617286	0.072486382714	1.68	0.982492785807	0.017507214193	2.09	0.996880460434	0.003119539566
1.28	0.929734182683	0.070265817317	1.69	0.983152585845	0.016847414155	2.10	0.997020533263	0.002979466737
1.29	0.931898614698	0.068101385302	1.70	0.983790457668	0.016209542332	2.11	0.997154844960	0.002845155040
1.30	0.934007929381	0.065992070619	1.71	0.984407006734	0.015592993266	2.12	0.997283606722	0.002716393278
1.31	0.936063109317	0.063936890683	1.72	0.985002826647	0.014997173353	2.13	0.997407023194	0.002592976806
1.32	0.938065143442	0.061934856558	1.73	0.985578499203	0.014421500797	2.14	0.997525292621	0.002474707379
1.33	0.940015016096	0.059984983904	1.74	0.986134593296	0.013865406704	2.15	0.997638606993	0.002361393007
1.34	0.941913706557	0.058086293443	1.75	0.986671669716	0.013328330284	2.16	0.997747152198	0.002252847802
1.35	0.943762188599	0.056237811401	1.76	0.987190273902	0.012809726098	2.17	0.997851108167	0.002148891833
1.36	0.945561430056	0.054438569944	1.77	0.987690941050	0.012309058950	2.18	0.997950649022	0.002049350978
1.37	0.947312385788	0.052687614212	1.78	0.988174194892	0.011825805108	2.19	0.998045943215	0.001954056785
1.38	0.949016024608	0.050983975392	1.79	0.988640547789	0.011359452211	2.20	0.998137153582	0.001862846418
1.39	0.950673286547	0.049326713453	1.80	0.989090500825	0.010909499175	2.21	0.998224437869	0.001775562131
1.40	0.952285111714	0.047714888286	1.81	0.989524543906	0.010475456094	2.22	0.998307948269	0.001692051731
1.41	0.953852432362	0.046147567638	1.82	0.989943155865	0.010056844135	2.23	0.998387831976	0.001612168024
1.42	0.955376172558	0.044623827442	1.83	0.990346804574	0.009653195426	2.24	0.998464231208	0.001535768792
1.43	0.956857247857	0.043142752143	1.84	0.990735947060	0.009264052940	2.25	0.998537283345	0.001462716655
1.44	0.958296565005	0.041703434995	1.85	0.991111029620	0.008888970380	2.26	0.998607121056	0.001392878944
1.45	0.959695021643	0.040304978357	1.86	0.991472487951	0.008527512049	2.27	0.998673872429	0.001326127571
1.46	0.961053506041	0.038946493959	1.87	0.991820747271	0.008179252729	2.28	0.998737661102	0.001262338898
1.47	0.962372892651	0.037627107349	1.88	0.992156222455	0.007843777545	2.29	0.998798606380	0.001201393620
1.48	0.963654059118	0.036345940882	1.89	0.992479318168	0.007520681832	2.30	0.998856823364	0.001143176636
1.49	0.964897859339	0.035102140661	1.90	0.992790429001	0.007209570999	2.31	0.998912423069	0.001087576931
1.50	0.966105141664	0.033894858336	1.91	0.993089939613	0.006910060387	2.32	0.998965512542	0.001034487458
1.51	0.967276743924	0.032723256076	1.92	0.993378224874	01006621775126	2.33	0.999016194979	0.000983805021
2.34	0.999064569837	0.000935430163	2.74	0.999893351284	0.000106648716	3.14	0.999991030434	0.000008969566
2.35	0.999110732946	0.000889267054	2.75	0.999899378076	0.000100621924	3.15	0.999991601789	0.000008398211
2.36	0.999154776621	0.000845223379	2.76	0.999905082351	0.000094917649	3.16	0.999992138259	0.000007861741
2.37	0.999196789766	0.000803210234	2.77	0.999910480287	0.000089519713	3.17	0.999992641873	0.000007358127
2.38	0.999236857979	0.000763142021	2.78	0.999915587315	0.000084412685	3.18	0.999993114550	0.000006885450
2.39	0.999275063657	0.000724936343	2.79	0.999920418146	0.000079581854	3.19	0.999993558102	0.000006441898
2.40	0.999311486091	0.000688513909	2.80	0.999924986804	0.000075013196	3.20	0.999993974239	0.000006025761
2.41	0.999346201572	0.000653798428	2.81	0.999929306653	0.000070693347	3.21	0.999994364578	0.000005635422
2.42	0.999379283478	0.000620716522	2.82	0.999933390426	0.000066609574	3.22	0.999994730645	0.000005269355
2.43	0.999410802377	0.000589197623	2.83	0.999937250253	0.000062749747	3.23	0.999995073881	0.000004926119
2.44	0.999440826109	0.000559173891	2.84	0.999940897685	0.000059102315	3.24	0.999995395645	0.000004604355

Table 6 (continued)

Error function $\mathbf{erf(x) = \frac{2}{\sqrt{\pi}} \int_0^x \exp(-y^2) dy}$

erfc(x) = 1-erf(x)

X	erf(x)	erfc(x)	X	erf(x)	erfc(x)	X	erf(x)	erfc(x)
2.45	0.999469419881	0.000530580119	2.85	0.999944343719	0.000055656281	3.25	0.999995697221	0.000004302779
2.46	0.999496646353	0.000503353647	2.86	0.999947598826	0.000052401174	3.26	0.999995979817	0.000004020183
2.47	0.999522565723	0.000477434277	2.87	0.999950672969	0.000049327031	3.27	0.999996244577	0.000003755423
2.48	0.999547235809	0.000452764191	2.88	0.999953575628	0.000046424372	3.28	0.999996492576	0.000003507424
2.49	0.999570712128	0.000429287872	2.89	0.999956315820	0.000043684180	3.29	0.999996724828	0.000003275172
2.50	0.999593047979	0.000406952021	2.90	0.999958902122	0.000041097878	3.30	0.999996942290	0.000003057710
2.51	0.999614294515	0.000385705485	2.91	0.999961342687	0.000038657313	3.31	0.999997145864	0.000002854136
2.52	0.999634500820	0.000365499180	2.92	0.999963645269	0.000036354731	3.32	0.999997336397	0.000002663603
2.53	0.999653713982	0.000346286018	2.93	0.999965817233	0.000034182767	3.33	0.999997514690	0.000002485310
2.54	0.999671979160	0.000328020840	2.94	0.999967865580	0.000032134420	3.34	0.999997681496	0.000002318504
2.55	0.999689339655	0.000310660345	2.95	0.999969796958	0.000030203042	3.35	0.999997837523	0.000002162477
2.56	0.999705836978	0.000294163022	2.96	0.999971617683	0.000028382317	3.36	0.999997983439	0.00000201656
2.57	0.999721510909	0.000278489091	2.97	0.999973333751	0.000026666249	3.37	0.999998119872	0.000001880128
2.58	0.999736399569	0.000263600431	2.98	0.999974950855	0.000025049145	3.38	0.999998247413	0.000001752587
2.59	0.999750539470	0.000249460530	2.99	0.999976474397	0.000023525603	3.39	0.999998366617	0.000001633383
2.60	0.999763965574	0.000236034426	3.00	0.999977909503	0.000022090497	3.40	0.999998478007	0.000001521993
2.61	0.999776711383	0.000223288617	3.01	0.999979261036	0.000020738964	3.41	0.999998582074	0.000001417926
2.62	0.999788808937	0.000211191063	3.02	0.999980533609	0.000019466391	3.42	0.999998679281	0.000001320719
2.63	0.999800288912	0.000199711088	3.03	0.999981731595	0.000018268405	3.43	0.999998770061	0.000001229939
2.64	0.999811180655	0.000188819345	3.04	0.999982859140	0.000017140860	3.44	0.999998854822	0.000001145178
2.65	0.999821512243	0.000178487757	3.05	0.999983920174	0.000016079826	3.45	0.999998933948	0.000001066052
2.66	0.999831310522	0.000168689478	3.06	0.999984918421	0.000015081579	3.46	0.999999007799	0.000000992201
2.67	0.999840601165	0.000159398835	3.07	0.999985857407	0.000014142593	3.47	0.999999076712	0.000000923288
2.68	0.999849408708	0.000150591292	3.08	0.999986740475	0.000013259525	3.48	0.999999141004	0.000000858996
2.69	0.999857756604	0.000142243396	3.09	0.999987570788	0.000012429212	3.49	0.999999200975	0.000000799025
2.70	0.999865667257	0.000134332743	3.10	0.999988351343	0.000011648657	3.50	0.999999256902	0.000000743098
2.71	0.999873162071	0.000126837929	3.11	0.999989084973	0.000010915027	3.51	0.999999309048	0.000000690952
2.72	0.999880261484	0.000119738516	3.12	0.999989774362	0.000010225638	3.52	0.999999357659	0.000000642341
2.73	0.999886985012	0.000113014988	3.13	0.999990422049	0.000009577951	3.53	0.999999402965	0.000000597035
3.54	0.999999445184	0.000000554816	3.70	0.999999832849	0.000000167151	3.85	0.999999948114	0.000000051886
3.55	0.999999484516	0.000000515484	3.71	0.999999845179	0.000000154821	3.86	0.999999952081	0.000000047919
3.56	0.999999521153	0.000000478847	3.72	0.999999856628	0.000000143372	3.87	0.999999955754	0.000000044246
3.57	0.999999555272	0.000000444728	3.73	0.999999867256	0.000000132744	3.88	0.999999959153	0.000000040847
3.58	0.999999587040	0.000000412960	3.74	0.999999877120	0.000000122880	3.89	0.999999962298	0.000000037702
3.59	0.999999616613	0.000000383387	3.75	0.999999886273	0.000000113727	3.90	0.999999965208	0.000000034792
3.60	0.999999644137	0.000000355863	3.76	0.999999894764	0.000000105236	3.91	0.999999967899	0.000000032101
3.61	0.999999669749	0.000000330251	3.77	0.999999902641	0.000000097359	3.92	0.999999970388	0.000000029612
3.62	0.999999693577	0.000000306423	3.78	0.999999909945	0.000000090055	3.93	0.999999972690	0.000000027310
3.63	0.999999715741	0.000000284259	3.79	0.999999916718	0.000000083282	3.94	0.999999974817	0.000000025183
3.64	0.999999736353	0.000000263647	3.80	0.999999922996	0.000000077004	3.95	0.999999976783	0.000000023217
3.65	0.999999755517	0.000000244483	3.81	0.999999928815	0.000000071185	3.96	0.999999978600	0.000000021400
3.66	0.999999773333	0.000000226667	3.82	0.999999934207	0.000000065793	3.97	0.999999980279	0.000000019721
3.67	0.999999789891	0.000000210109	3.83	0.999999939202	0.000000060798	3.98	0.999999981829	0.000000018171
3.68	0.999999805277	0.000000194723	3.84	0.999999943829	0.000000056171	3.99	0.999999983261	0.000000016739
3.69	0.999999819571	0.000000180429						

temperature for the copper-gilded coronet ranged from 240 to 285 ℃. By analyzing the distribution of copper, it was determined that the diffusion depth of Cu atoms due to heat-driven diffusion was less than 2 μm. Previous research indicated that the heating time for copper gilding was approximately 15 min. The calculated diffusion distance, based on Fick's second law, aligned with the diffusion behavior of copper atoms along defects at temperatures ranging from 240 to 285 ℃. These findings confirmed that the copper crown underwent gilding at a temperature of 240 to 280 ℃ for a duration of 15 min. Therefore, the formation mechanism of the gold layer involved the solid-state phase transformation of the gold amalgam. Moreover, the gold layer was securely attached to the substrate through defect-assisted diffusion of Cu atoms.

Nevertheless, it is essential to acknowledge that the phenomenon of copper diffusion during heating in gilding processes has rarely been reported, primarily due to the long-term corrosion diffusion of the copper substrate. Fortunately, this study successfully estimated the diffusion distance of Cu during heating based on the concentration distribution of Cu. As a result, the heating temperature of the gilding process was inferred using the phase transformation law of the Au-Cu system and further validated by the diffusion law of copper. This research endeavor is anticipated to offer novel ideas and insights into the investigation of the technological process and formation mechanism of ancient copper gilding techniques.

Abbreviations

XRF	X-ray fluorescence
SEM–EDS	Scanning electron microscope with energy dispersive spectrometer
BSE	Backscattered electron
XRD	X-ray diffraction
XPS	X-ray photoelectron spectroscopy
Au	Gold
Ag	Silver
Hg	Mercury
Cu	Copper
O	Oxygen
Cl	Chlorine

Acknowledgements
We would like to thank the Xi'an Institute of Conservation and Archaeology on Cultural Heritage for the samples. The authors are grateful to Ms. Juan Ji from Shaanxi Institute for the Preservation of Cultural Heritage, for the support and help on the metallographic investigation, and SEM-EDS. Special thanks go to Zhuoyan Tuoba and Lifeng Jiang for suggestions on the manuscript. We also appreciate the valuable comments from the four anonymous reviewers, Editorial Board Member, and in-house Editor.

Author contributions
YS: Methodology, Validation, Investigation, Data analyses, Writing—original draft, Writing—review and editing. FJ: Methodology, Project administration. Writing—review and editing. JY: Methodology, Project administration. QZ: Project administration, Excavation and restoration of cultural relics. XL; Wenbin Fu and SY: Methodology. All authors read and approved the final manuscript.

Funding
The Project Supported by. The Humanities and Social Sciences Foundation of Ministry of Education of China (No. 21YJCZH050). Natural Science Basic Research Program of Shaanxi (Program No. 2021JQ105). Scientific Research Project of Shaanxi History Museum (Program No. GJ2021007). The Fundamental Research Funds for the Central Universities (Social Sciences), Northwestern Polytechnical University (No. D5000210802).

Availability of data and materials
The data and materials used during the study are available from the corresponding author on reasonable requests.

Declarations

Consent to participate
Not applicable.

Competing interests
The authors declare that they have no competing interests.

Received: 22 February 2023 Accepted: 17 July 2023
Published online: 31 July 2023

References

1. Liu Y, Li R, Yang JC, et al. China and the steppe: technological study of precious metalwork from Xigoupan Tomb 2 in the Ordos region. Inner Mongolia Heritage Sci. 2021. https://doi.org/10.1186/s40494-021-00520-5.
2. Liu Y. Lacquerware from the tomb of Marquis. Haihun. 2019;50(3):232.
3. Giumlia-Mair A. Plating and surface treatments on ancient metalwork. Adv Archaeomater. 2020;1(1):1–26.
4. Gard FS, Daizo MB, Santos DM, et al. Application of surface science techniques to study a gilded Egyptian funerary mask: a multi-analytical approach. Surf Interface Anal. 2019;51(10):1001–17.
5. Liu Y, Yang JC, Tan PP. Some new thoughts about the technologies of "*Cuojinyin*". Sci Conserv Archaeol. 2019;031(004):75–86.
6. Darque-Ceretti D, Marc Aucouturier EF. Foil and leaf gilding on cultural artifacts. Forming and adhesion Revista Matéria. 2011;16(1):540–59.
7. Shao YB, Lu X, Fu WB, et al. Technical characteristics and coating formation mechanism of gilded silver products unearthed from the consort tomb of emperor *Shengzong* of the *Liao* Dynasty. Archaeol Anthropol Sci. 2023. https://doi.org/10.1007/s12520-023-01725-4.
8. Ynsa MD, Chamón J, Gutiérrez PC, Gomez-Morilla I, Enguita O, Pardo AI, Arroyo M, Barrio J, Ferretti M, Climent-Font A. Study of ancient Islamic gilded pieces combining PIXE-RBS on external microprobe with SEM images. Appl Phys. 2008;92(1):235–41.
9. Sparavigna AC. Depletion gilding: An ancient method for surface enrichment of gold alloys. Mechan Mater Sci Eng. 2016
10. Leusch V. On the invention of gold metallurgy: The gold objects from the varna I cemetery (Bulgaria)-technological consequence and inventive creativity. Camb Archaeol J. 2015;25(01):353–76.
11. Gao XS. A research of gold-plating technique- starting with gold-plated bronzed wares found in *Luoyang*. Journal of Luoyang Normal Univ. 2019;028(006):23–6.
12. Jin PJ, Ruan F, Yang X, et al. Microstructural and componential characterization of the plating technology on Chinese *Han* dynasty bronze fragments. Archaeometry. 2017;59(2):274–86.
13. Zhao JY, Liu R, Lv Y. Interviews with elements Femme Fatal mercury. University Chemistry. 36(10) 39–40
14. Oddy WA. Gilding of metals in the old world. Metal Plating Patination. 1993. https://doi.org/10.1016/B978-0-7506-1611-9.50019-4.
15. Strub E. Investigation on fire gilding using XRF and NAA, in NRC-9. 2016. Helsinki, Finland.
16. Ottenwelter E, Josse C, Proietti A, et al. Fire gilding investigation on early medieval copper-based jewellery by focused ion beam (FIB) on FEG-SEM. J Archaeol Sci Rep. 2022. https://doi.org/10.1016/j.jasrep.2022.103602.

17. Bayley J, Russel A. Making gold-mercury amalgam: The evidence for gilding from Southampton. Antiqu J. 2008;88:37–42.
18. Oddy WA. Gilding: An outline of the technological history of the plating of gold on to silver or copper in the old world. Endeavour. 1991.
19. Chudnenko K, Pal'yanova G. Thermodynamic properties of Au-Hg binary solid solution. Thermochimica Acta. 2013;566:175–80.
20. Ji J, Ma LY, Bai K, et al. Analysis of *Bajunshoucheng* gilding bronze seal of the Eastern *Han* dynasty in Guizhou by scanning electron microscope. J Chin Electron Microsc Soc. 2019;38(01):51–5.
21. Shemakhanskaya M, Treister M, Yablonsky L. The technique of gold inlaid decoration in the 5th-4th centuries BC: silver and iron finds from the early Sarmatian barrows of Filippovka. Southern Urals Archéo-Sciences. 2009;33:211–20.
22. Margreiter R, Bauman J, Mantouvalou I, et al. Investigations on fire-gilding. Archaeometry. 2022;64(6):1465–78.
23. Crina Anca Sandu I, Sá Helena M, CostaPereiraPereira M. Ancient 'gilded' art objects from European cultural heritage a review on different scales of characterizatio. Surf Interface Anal. 2011;43(8):1134–51.
24. Corregidor V, Alves LC, Barradas NP, et al. Characterization of mercury gilding art objects by external proton beam. Nucl Instrum Methods Phys Res, Sect B. 2011;269(24):3049–53.
25. Ingo GM, Riccucci C, Pascucci M, et al. Combined use of FE-SEM+EDS, ToF-SIMS, XPS, XRD and OM for the study of ancient gilded artefacts. Appl Surf Sci. 2018;446:168–76.
26. Cesareon R. Gold, gildings, and tumbaga from the Moche tomb of the Lady of Cao: An EDXRF test for the internal ratio method. X-Ray Spectrom. 2019;48(3):202–7.
27. Deng L, Ouyang X, Jin J, et al. Exploiting the higher specificity of silver amalgamation Selective detection of mercury (II) by forming Ag/Hg amalgam. Anal Chem. 2013;18:8594–600.
28. Anheuser K. The practice and characterization of historic fire gilding techniques. Archaeotechnology. 1997;49(11):58–62.
29. Sun J. Gold and silver metallurgy. Dongcheng: Metallurgical Industry Press; 1986.
30. McCann L, Trentelman K, Possley T, et al. Corrosion of ancient Chinese bronze money trees studied by Raman microscopy. J Raman Spectrosc. 1999;30(2):121–32.
31. He L, Liang JY, Zhao X, et al. Corrosion behavior and morphological features of archeological bronze coins from ancient China. Microchem J. 2011;99(2):203–12.
32. Bernard MC, Joiret S. Understanding corrosion of ancient metals for the conservation of cultural heritage. Electrochim Acta. 2009;54(22):5199–205.
33. Mead H, Birchenall CE. Diffusion in gold and Au-Ag alloys. JOM. 1957;9(7):874–7.
34. Ma QL, Scott D. Gold and silver gilding techniques in the Western Han Dynasty of China. Sci Conserv Archaeol. 2004;16(2):21–6.
35. Ravi R, Paul A. Diffusion mechanism in the gold-copper system. J Mater Sci: Mater Electron. 2012;23(12):2152–6.
36. He YA, Shao L. Chinese gold and silver ware. Beijing: Central Compilation & Translation Press, 2010: 77–106
37. Tan PP, Yang JC, Ren XL. Technical Features of A Ninth-Century Silver Vessel of Southern China Uncovered From Famen Monastery, Shaanxi Province. Heritage Science. 2021.
38. Gao XS. A preliminary study on gilded wares of Warring States Period and related issues. Journal of National Museum of China. 2012. 000(004): 42–55
39. Shao YB, Jiang FR, Du JN, et al. Brass products in the coronet excavated from an M2-numbered Sui-Tang-dynasty tomb situated in *Kun Lun* Company in. Xi'an Herit Sci Shaanxi. 2021. https://doi.org/10.1186/s40494-021-00625-x.
40. Shaanxi Institute of Archaeology. Summary of archaeology of the Three Kingdoms, Sui, Tang, Song, Yuan, Ming and Qing Dynasties in Shaanxi from 2008 to 2017. Archaeol Cult Relics. 2018;5:111–47 ((**In Chinese**)).
41. Tan PP, Yang JC, Zheng YZ, et al. Copper granulation: scientific analysis on the ornaments from the coronet of Lady Pei of the early Tang Dynasty (618–712 AD) in Xi'an. Shaanxi China Archaeol Anthropol Sci. 2019;11(12):6603.
42. Gu MY. Study on the crown of noble women in Sui and Tang dynasties. Xi'an: Shaanxi Normal University; 2018.
43. Palsson N, Khamsuk P, Sorachot S, et al. Corrosion behavior of zinc and copper coated structural steels in soil environments. Materialwiss Werkstofftech. 2022;53(1):68–79.
44. De Ryck I, Van Biezen E, Leyssens K, et al. Study of tin corrosion: the influence of alloying elements. J Cult Herit. 2004;5(2):189–95.
45. Han MS, Hwang JJ, Moon WS. A study on the production techniques of ancient gilding-Focus on the mercury amalgam gilding. Scientific Research on Conservation. 2002: 113–129
46. Ingo GM, Angelini E, Bultrini G, et al. Study of long-term corrosion layers grown on high-tin leaded bronzes by means of the combined use of GDOES and SEM + EDS. Surf Interface Anal. 2002;34(1):337–42.
47. Wang J, Qin HB, Chen JF, et al. First-principles study on the elastic mechanical properties and anisotropies of gold-copper intermetallic compounds. Metals. 2022. https://doi.org/10.3390/met12060959.
48. Ma X, Shen Y, Yao S, et al. Self-supported nanoporous Au3Cu electrode with enriched gold on surface for efficient electrochemical reduction of CO2. Chem A Eur J. 2020;26(18):4143–9.
49. Wang Z, Huang L, Zhang M, et al. Chemical mechanism-dominated and reporter-tunable surface-enhanced raman scattering via directional supramolecular assembly. J Am Chem Soc. 2022;144(38):17330–5.
50. Liu S, Xu Y, Jiao S, et al. Rational construction of Au_3Cu@ Cu nanocages with porous core–shell heterostructured walls for enhanced electrocatalytic N_2 fixation. J Mater Chem A. 2021;9(13):8372–7.
51. Akitsu T. Using XRD technique for model composite and related materials. In: Nanotechnology in the automotive industry. Amsterdam: Elsevier; 2022. p. 15–35.
52. Madakson P, Liu JC. Interdiffusion and resistivity of Cu/Au, Cu/Co, Co/Au, and Cu/Co/Au thin films at 25–550 °C. J Appl Phys. 1990;68(5):2121–6.
53. Ravi R, Paul A. Diffusion mechanism in the gold-copper system. J Mater Sci Mater Electron. 2012;23(12):2152–6.
54. Fedorov PP, Volkov SN. Au-Cu phase diagram. Russ J Inorg Chem. 2016;61(6):772–5.
55. Okamoto H, Chakrabarti DJ, Laughlin DE, et al. The Au-Cu (gold-copper) system. J Phase Equil. 1987;8(5):454–74.
56. Hennig J, Mari D, Schaller R. Order-disorder phase transition and stress-induced diffusion in Au-Cu. Phys Rev B. 2009;79(14): 144116.
57. Wang M, Zheng SQ, Duan Y. 2001. Treatment of mercury and its containing waste liquid in the laboratory. Heilongjiang Med Pharm. 2001. 85
58. Okamoto H, Massalski TB. The Au-Hg (gold-mercury) system. Bull Alloy Phase Diagrams. 1989;10(1):50–8.
59. Pinnel MR, Bennett JE. On the formation of the ordered phases CuAu and Cu_3Au at a copper/gold planar interface. Metall Trans A. 1979;10(6):741–7.
60. Pinnel MR. Diffusion-related behaviour of gold in thin film systems. Gold Bull. 1979;12(2):62.
61. Khobaib M, Gupta KP. Duffusion of Cu in AuCu alloy. Scr Metall. 1970;4:605–10.
62. Mello E, Di Paola E, Marra G, et al. Advances in materials and technological characterization of Lorenzo Ghiberti's Gates of Paradise. Eur Phys J Plus. 2021. https://doi.org/10.1140/epjp/s13360-021-01851-9.
63. Ohring M. Materials science of thin films. Cambridge: Academic Press; 2002.
64. Shewmon P. Diffusion in solids. Chicago: McGraw-Hill; 1988.
65. Khobaib M, Gupta KP. Diffusion of Cu in AuCu alloy. Scr Metall. 1970;4(8):605–9.
66. Pan JD, Balluffi RW. Diffusion-induced grain-boundary migration in Au/Cu and Au/Ag thin films. Unknown. 1982;30(4):861–70.
67. Tian Y, Zhang C, Lei Z, et al. An improved multicomponent diffusion model for compositional simulation of fractured unconventional reservoirs. SPE J. 2021;26:1–26.
68. Caraballo T, López-De-La-Cruz J, Rapaport A. Study of the dynamics of two chemostats connected by Fickian diffusion with bounded random fluctuations. Stochast Dynam. 2022. https://doi.org/10.1142/S0219493722400020.
69. D'Heurle FM, Gas P, Philibert J. Diffusion—reaction: the ordered Cu_3au rule and its corollaries. Solid State Phenom. 1995;41:93–102.

Publisher's Note